Spatio-Temporal Progression of Two-Stage Autoignition for Diesel Sprays in a Low-Reactivity Ambient: n-Heptane Pilot-Ignited Premixed Natural Gas

Author, co-author (Do NOT enter this information. It will be pulled from participant tab in MyTechZone)

Affiliation (Do NOT enter this information. It will be pulled from participant tab in MyTechZone)

Abstract

The spatial and temporal locations of autoignition depend on fuel chemistry and the temperature, pressure, and mixing trajectories in the fuel jets. Dual-fuel systems can provide insight into fuel-chemistry aspects through variation of the proportions of fuels with different reactivities, and engine operating condition variations can provide information on physical effects. In this context, the spatial and temporal progression of two-stage autoignition of a diesel-fuel surrogate, *n*-heptane, in a lean-premixed charge of synthetic natural gas (NG) and air is imaged in an optically accessible heavy-duty diesel engine. The lean-premixed charge of NG is prepared by fumigation upstream of the engine intake manifold. Optical diagnostics include: infrared (IR) imaging for quantifying both the in-cylinder NG concentration and the pilot-jet penetration rate and spreading angle, high-speed cool-flame chemiluminescence imaging as an indicator of low-temperature heat release (LTHR), and high-speed OH* chemiluminescence imaging as an indicator high-temperature heat release (HTHR). To aid interpretation of the experimental observations, zero-dimensional chemical kinetics simulations provide further understanding of the underlying interplay between the physical and chemical processes of mixing (pilot fuel-jet entrainment) and autoignition (two-stage ignition chemistry). Increasing the premixed NG concentration prolongs the ignition delay of the pilot fuel and increases the combustion duration. Due to the relatively short pilot-fuel injections utilized, the transient increase in entrainment near the end of injection (entrainment wave) plays an important role in mixing. To achieve desired combustion characteristics, i.e., ignition and combustion timing (e.g., for combustion phasing) and location (e.g., for reducing wall heat-transfer or tailoring charge stratification), injection parameters can be suitably selected to yield the necessary mixing trajectories that potentially help offset changes in fuel ignition chemistry, which could be a valuable tool for combustion design.

Introduction

To comply with increasingly stringent scrutiny and regulation of heavy-duty vehicle exhaust emissions and to meet the ever-increasing energy demands for both transportation and stationary applications, natural gas (NG) is an alternative fuel option for internal combustion (IC) engines. The combustion of lean premixed NG in IC engines is a promising alternative to diesel operation due to lower CO_2 emissions, significantly reduced particulate (soot) and NOx emissions, and high knock (autoignition) resistance enabling diesel-like compression ratios to achieve diesel like efficiencies [1, 2]. Despite lean-premixed combustion of NG offering improved knock resistance, the low chemical reactivity of NG presents significant challenges in reliable ignition and progression of combustion through lean mixtures. Consequently, unburned hydrocarbon (UHC) emissions, combustion instability, and tendency to misfire are increased. To overcome these difficulties, advanced ignition systems like pilot-fuel injections [3, 4] or pre chamber spark-ignition [5, 6] can be utilized to promote stable and rapid combustion.

In pilot-fuel injection ignition systems, combustion is initiated by a small injection of a high cetane-number (high-reactivity) liquid fuel, typically diesel fuel, into a low-reactivity fuel-lean premixed charge of NG. The spatial and temporal location of the resulting autoignition is governed by the interaction between the physical effects related to mixing of the pilot fuel-jet with the premixed NG charge and chemical effects of autoignition reactions in the local mixtures of the two fuels. Previous studies utilizing this 'Diesel-piloted dual-fuel (DPDF) combustion' approach have reported a tradeoff between low UHC emissions and low NO_x and soot emissions. Increased pilot-fuel mass results in more complete combustion of the premixed NG charge, but soot and NO_x emissions tend to increase [1,2]. Conversely, with lower pilot-fuel mass, combustion performance tends to deteriorate due to the high sensitivity of ignition delay to changes in premixed NG concentration [1], which leads to large cycle-to-cycle variations and increasing tendency to misfire. Fundamental understanding of the underlying interplay between the physical and chemical processes of mixing (pilot fuel-jet entrainment) and autoignition (two-stage ignition chemistry) is important for designing DPDF combustion systems that reliably achieve and control ignition in lean-burn premixed NG engines. Due to the ignition-inhibiting effects of NG on n-heptane ignition, the interplay between mixing and the progression of first-stage and second-stage ignition reactions will be increasingly important as the main chamber NG concentration is increased.

Dual-fuel combustion of the pilot-fuel in a premixed-lean NG mixture is complicated by multiple degrees of stratification: temperature stratification due to pilot-fuel vaporization-cooling, equivalence-ratio stratification due to partial mixing of the pilot-fuel, and reactivity stratification due to local variations in the ratio of high reactivity pilot-fuel to low reactivity NG. DPDF combustion as such progresses through several overlapping stages, from a short transient pilot-fuel injection into a premixed NG fuel-air mixture, to autoignition of the pilot-fuel and entrained NG, to combustion of NG in the immediate vicinity of the burning pilot jet, and finally to sequential autoignition and/or premixed turbulent flame propagation of the remaining premixed NG. Apart from conventional metal-engine experiments, only a few studies conducted with optical access have provided

imaging of dual-fuel combustion processes. Prior optical investigations of dual-fuel combustion have mostly focused on the detection of ignition delay [3,4], flame luminosity [4-7] and sooting propensity [6]. These studies reported a considerable increase in the ignition delay of the pilot-fuel in the presence of a premixed NG mixture [1,3,4,7]. Furthermore, fundamental studies on the two-stage autoignition behavior of fuels under diesel-engine conditions have received considerable attention in the recent years [8-11]. Nonetheless, fundamental understanding of the interaction between mixing and inhibitive effect of NG on the two-stage autoignition behavior of diesel-like fuels is still rather limited. Thus, the overarching goal of this work is to shed light on the interplay between the physical and chemical processes that govern ignition of pilot-injections in the context of dual-fuel combustion.

Dual Fuel Combustion Processes

DPDF ignition and combustion characteristics are controlled by the mixing rate and ignition chemistry of the pilot-fuel as well as by the concentration of the low-reactivity, premixed lean NG mixture inside the cylinder. The heat release characteristics in a typical DPDF combustion mode are governed by the interaction between the physical and chemical processes of mixing and autoignition.

The fumigation of NG into the intake stream causes variations in the physical and transport properties of the mixture, such as the specific heat ratio and to a lesser extent the heat transfer parameters [12]. Furthermore, the reduced oxygen intake partial pressure (due to the displacement of air by NG), the inhibitive effect of NG on the pre-ignition (cool-flame) reactivity of the pilot-fuel, along with changes to the associated heat release and change in the residual gas composition (significant only for continuous engine operation, not relevant for skip-fire operation employed in the study) can cause significant changes in the progress of pre-ignition processes of the pilot-fuel thereby resulting in longer ignition delay period [13-15].

During the course of the compression stroke, the temperature and pressure of the premixed NG fuel-air mixture increases. Even in the absence of pilot-fuel, certain pre-ignition reactions may progress significantly within the NG fuel-air mixture, even under lean conditions ($\phi_{NG} > 0.3$), which can further increase temperatures [16]. For constant intake-temperature conditions, this additional increase in temperature can compensate for the minor lowering of the charge temperature caused due to changes in the thermodynamic properties (specific heat ratio) of the charge when premixed NG is added to air [17]. These pre-ignition reactions may produce some partial-oxidation products such as radicals, aldehydes, and CO, which can build up to significant concentrations during the latter part of the compression stroke, thereby influencing the ignition and subsequent combustion processes of the injected pilot-fuel. This contributes directly to both combustion of NG entrained into pilot-fuel and in its immediate vicinity and combustion of NG well outside the jets. Of course, turbulent flame propagation initiated by pilot-fuel ignition will not proceed throughout the premixed charge of NG outside the pilot jets unless the concentration of NG is high enough to sustain flame propagation [18].

Thus the overall heat release in DPDF combustion mode is essentially composed of three over-lapping mechanisms: (i) the combustion of the pilot-fuel jet and entrained NG, (ii) the combustion of NG in the immediate vicinity of the ignited pilot-fuel jet that allows for partial-flame propagation due to sustained thermal and mass transfer from the burning pilot-fuel jet, and (iii) the subsequent sequential autoignition and/or turbulent flame propagation within the overall lean mixture outside the pilot jets. During the mixing-controlled combustion phase of the pilot-fuel, the location and extent of the non-premixed flame determined by the stoichiometry envelope ($\phi_{overall} = 1.0$) is shifted outward with increasing premixed NG concentration. With premixed NG fuel-air mixtures that are below the lean flammability limit, the bulk of the heat release is due to the ignition and subsequent rapid combustion of the pilot-fuel jet along with some entrained NG. It can also be due to combustion of NG in the immediate surroundings of the burning pilot-fuel jet that are now characterized by the presence of richer mixture regions (compared to pilot-fuel only case) and attaining higher temperatures due to thermal and mass transfer from the burning pilot-jet. The spatial extent of this region and its associated heat release might be manipulated by adjusting the quantity of injected pilot-fuel and/or the injection parameters (fuel-rail pressure and DSE). This can affect the tip penetration rate (fuel-rail pressure) and the mixing trajectory (DSE controls the timing of end of injection (EOI) and associated transient changes to entrainment) of the pilot-fuel which controls the total amount of NG entrained, and the extent of partial flame-propagation (flame spread) in the NG fuel-air mixture. On the other hand, increasing the premixed NG concentration will eventually allow for flame propagation and/or sequential autoignition through the premixed NG charge outside the pilot-fuel jet. This also results in increasing overlap between the heat release during the second and third phases of combustion.

Experimental Overview

Optical Engine

The experiments use the Sandia-Cummins single-cylinder heavy-duty optical engine, which is modified from a single-cylinder Cummins N-series direct-injection, heavy-duty diesel engine. The optical engine has a 13.97-cm bore and 15.24-cm stroke, yielding a displacement of 2.34 L per cylinder. The intake-port geometry of the production engine, which has a steady-state (i.e., measured on a flow-bench) swirl ratio of 0.5 [19], is preserved in the optical engine. The engine is equipped with a Bowditch piston with an open, right-cylindrical bowl and a flat fused-silica piston-crown window to allow optical access to the bowl, viewing from below. Further, one of the two exhaust valves has been replaced with a window, which provides a view of the squish region from above (this view not used in this study). Flat rectangular windows installed in a ring at the top of the cylinder provide additional laser access through the cylinder wall. Further details about this engine can be found elsewhere [20,21]. A schematic layout of the optical engine with the imaging setups are shown in Figure 1, and the major specifications of the engine and fuel injector are tabulated in Table 1.

Fuel Injection Systems

A Delphi DFI 1.5 light-duty, solenoid-actuated common-rail injector with eight equally spaced 0.131-mm orifices is used for its fast response time and its ability to deliver consistent, short-duration pilot injections. The pilot fuel is high purity n-heptane (≥99% high-performance liquid chromatography grade, from MilliporeSigma), which is selected for its low fluorescence upon illumination by ultraviolet (UV) laser-light, while retaining ignition properties typical of diesel fuel.

A Clean Air SP010, solenoid-actuated, single-hole gas injector fitted on the intake manifold 0.55 m upstream of the intake engine port fumigates the NG into the intake air stream using a perforated annular tube embedded in the intake flow. The location of the NG fumigation injector coupled with the long residence time from injection to induction into the engine (4-5 cycles) yields a relatively homogenous

premixed NG-air charge. Additionally, a modified GM LT4 GDI injector is mounted in the cylinder wall for direct injection of natural gas into the combustion chamber, which is used here for fueling calibration purposes only. The NG is a synthetic mixture of 95% methane, 4% ethane, and 1% propane by volume.

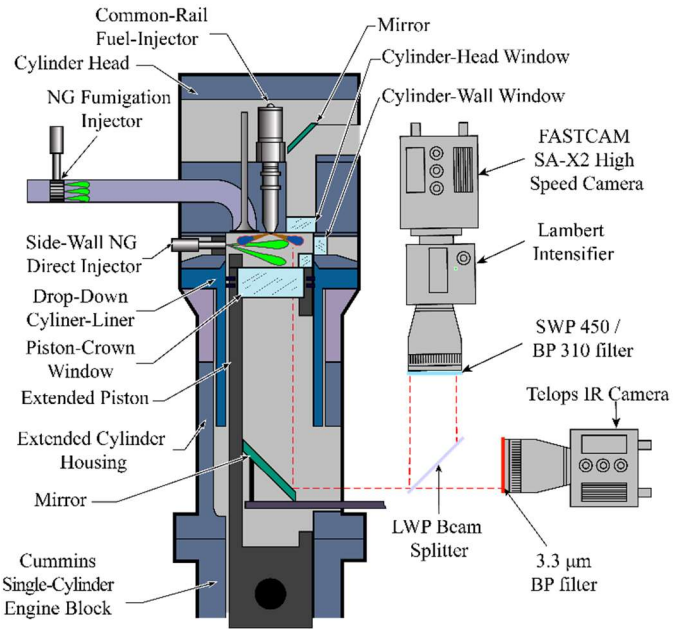

Figure 1. Schematic layout of the optical engine and imaging setup.

Optical Engine Diagnostics

Several diagnostics measure the spatial and temporal autoignition characteristics of n-heptane in the presence of natural gas, including cylinder-pressure measurements and three different optical diagnostics. Cylinder pressure is measured with an AVL QC34D piezoelectric pressure transducer and recorded every quarter crank angle degree. The apparent heat release rate is calculated from the measured cylinder pressure using standard techniques [22] without accounting for any heat losses. Before computing the AHRR, the cylinder pressure data are smoothed using a Fourier-series low-pass filter with a Gaussian roll-off function having a 100% transmission between from 0 to 800 Hz and dropping to 1% at 3360 Hz. Due to the relatively slow energy release at the operating conditions investigated here, the filtering scheme removes acoustic ringing with virtually no effect on the shape of the AHRR curve [23].

To quantify the in-cylinder NG concentration and to characterize the n-heptane jet (tip penetration, spreading angle), infrared (IR) C-H stretch emission images are captured by a Telops TS-IR MW InSb camera fitted with a Spectrogon band-pass filter (BPF) centered at 3.317 micrometers with 215 nm full width at half-maximum (FWHM). The BPF transmits IR emission from both NG and n-heptane arising from C-H vibrational stretching at elevated in-cylinder temperatures achieved during compression prior to combustion, as well as during combustion. The exposure time and resolution of the IR camera are set to 40 µs and 640×512 pixels, respectively. Due to the slow framing rate of the IR camera, only one IR image is acquired every cycle.

Table 1. Engine and injector specifications.

Engine Specifications	
Engine base type	Cummins N-14, DI diesel
Number of cylinders	1
Number of intake valves	2
Number of exhaust valves	1*
Combustion Chamber	Quiescent, direct injection
Swirl ratio	0.5
Bore × Stroke [cm]	13.97 × 15.24
Bowl Width, Depth [cm]	9.78, 1.55
Displacement [liters]	2.34
Connecting rod length [cm]	30.48
Natural Gas Fumigation Injector Specifications	
Fuel injector type	Solenoid actuated, Clean Air SP010 Gas Injector
Number of holes	1
Fuel	Natural gas (95% CH_4, 4% C_2H_6 1% C_3H_8 by vol.)
Natural Gas Side Injector Specifications	
Fuel injector type	Solenoid actuated, modified GM LT4 GDI
Number of holes	1 × 1 mm diam.
Fuel	Natural gas (95% CH_4, 4% C_2H_6 1% C_3H_8 by vol.)
Pilot Fuel Injector Specifications	
Fuel injector type	Common Rail, solenoid actuated Delphi DFI 1.5
Orifices and diameter [mm]	8 equally-spaced, 0.131
Included spray angle	156°
Fuel	n-heptane

* In this optically accessible diesel engine, one of the two exhaust valves of the production cylinder head is replaced by a window.

Two different chemiluminescence imaging techniques provide insight into the spatial and temporal autoignition characteristics of the transient n-heptane jets injected into premixed natural gas. Crank-angle resolved non-simultaneous first-stage, cool-flame (broadband blue) chemiluminescence [24] and second-stage, high-temperature filtered OH* chemiluminescence [25] images are captured by a Photron FASTCAM SA-X2 high speed camera coupled to a Lambert Hi-CATT high-speed intensifier with a S-20 photocathode. The exposure time and resolution of the high-speed camera are set to 50 µs and 768×768 pixels, respectively. The high-speed images are captured every 0.5°CA. The gate width and the gain of the intensifier are set 50 µs and 80% respectively. The first stage, cool-flame chemiluminescence images are captured with a 105 mm glass (visible) Nikkor lens with a fully open aperture (f/2.8) and a 415-440 nm BPF. This BPF and glass lens reject chemiluminescence from the ultra-violet (UV) range (i.e., OH* does not contribute to the cool-flame images presented). Furthermore, the filter also rejected long-wavelength (green through IR) soot luminosity. Hence, the recorded first-stage luminosity is most likely dominated by chemiluminescence from HCHO*, HCO*, CH*, CO_2*, and/or broadband emission from the CO continuum [26,27]. The second-stage, high-temperature ignition, as indicated by OH* chemiluminescence, is imaged using a 105 mm UV Nikkor lens with the aperture set between f/4.5 and f/22 depending on experimental conditions to avoid saturation, and in combination with a 310-nm BPF with a 10-nm FWHM.

This combination of blue-visible and UV chemiluminescence imaging tracks the spatial and temporal evolution of two important excited

species produced during autoignition, formaldehyde (HCHO*) and the hydroxyl radical (OH*), respectively, which provide information about the two-stage autoignition of n-heptane-NG mixtures under these experimental conditions. Excited-state formaldehyde is produced during first-stage, low-temperature ignition and is consumed during second-stage, high-temperature ignition. OH* is produced during the second-stage, high-temperature ignition and provides an indication of both second-stage ignition and subsequent evolution of both mixing-controlled and flame-propagation/distributed-ignition combustion that follows. Note that although a small amount of OH* is likely produced during first-stage ignition, its concentration rises by orders of magnitude at second-stage ignition [24]. Also, the relatively narrow 310-BPF helps to isolate OH* from other emission sources, but some strong emission, likely from luminous soot, can interfere with the OH* signal for some conditions, as will be shown in the results section.

Engine Operating Conditions and Test Matrix

The optical engine is operated in "9:1 skip-fire" mode to avoid excessive temperature gradients within the optical windows that could cause them damage. That is, nine motored cycles precede each fired cycle. Each experimental test run consists of 30 fired cycles after the engine is motored for 60 seconds at constant speed. The salient operating conditions of the engine along with the test matrix are tabulated in Table 2. The start of solenoid energizing (SSE) time for the pilot-fuel injections is held constant for all experiments at 347 crank-angle degrees (CAD), with 360 CAD defined as top dead-center (TDC) of the compression stroke. From the IR images, the real start of injection (SOI), when fuel first emerges from the injector nozzles, was determined to be approximately 2.5 degrees crank angle (ºCA). This dwell between SSE and SOI is due to electromechanical and hydraulic delays inside the injector. The engine is operated at constant speed of 1200 rotations per minute (RPM). As specified in Table 2, three different pilot-fuel injection parameter combinations of fuel-rail pressure and duration of solenoid energization (DSE) are studied: 800 bar and 500 µs; 400 bar and 760 µs; and 800 bar and 760 µs. We chose these combinations so that the data could be compared on the basis of equal pilot fuel mass (#1 and #2), identical DSE (#2 and #3) and identical fuel-rail pressure (#1 and #3). Additionally, at a given pilot-fuel injection parameter combination, premixed NG-air concentrations (before pilot-fuel injection) is varied between a natural gas equivalence ratio (ϕ_{NG}) of zero (no n-heptane, air only) to $\phi_{NG} = 0.5$, in steps of 0.1.

Table 2. Experimental conditions and test case specifications.

Experimental Conditions			
Intake Temperature [ºC]	100		
Intake O_2 [%] (N_2 dil.)	21		
NG Port Injector Pressure [bar]	7.5		
NG Port Injector SSE [CAD]	40		
NG Port Injector DSE [ms]	3 - 23		
Pilot fuel	n-heptane		
Engine speed [RPM]	1200		
gIMEP [bar]	0.2 - 12		
Intake Pressure [kPa]	100		
Test Case Specifications			
Parameters	Test Series 1	Test Series 2	Test Series 3
Fuel-Rail Pressure [bar]	800	400	800
Pilot DSE [µs]	500	760	760
Pilot SSE [CAD]	347	347	347
Pilot SOI [CAD]	349.5	349.75	349.5
Pilot DOI [µs]	625	868	1181
Pilot EOI [CAD]	354	356	358
Pilot-fuel mass [mg]	11.5	11.5	24.3
ϕ_{NG} (before pilot)	0.0 (n-heptane pilot only), 0.1, 0.2, 0.3, 0.4, 0.5		
Test Series #1 and #2: Equal pilot fuel mass Test Series #2 and #3: Identical DSE Test Series #1 and #3: Identical fuel-rail pressure			
SOI Charge Conditions			
ϕ_{NG}	Pressure [bar]	Temperature [K]	
0.0	21.75	871.4	
0.5	21.75	849.1	

Chemical Kinetics Simulation

The chemical kinetics of n-heptane autoignition in the presence of natural gas are simulated to better understand the experimental data. These simulations are not intended to predict all of the in-cylinder processes, but rather to isolate the chemical effects of variations of the premixed NG concentration on the ignition delay in canonical scenarios to aid interpretation of experimental data. While higher-fidelity combustion models that capture both fluid-mechanic and chemical processes could be used in conjunction with an experiment like the one described here, the simple homogeneous reactor model decouples chemistry from other simultaneous processes, leading to a more straightforward parametric understanding of in-cylinder effects.

The simulations use a zero-dimensional (0-D) homogeneous reactor model initialized at estimated in-cylinder temperatures and pressures across a range of n-heptane concentrations that exist within the jets. The pressure and temperature at SOI are estimated based on isentropic compression of NG-air mixtures assuming frozen composition. To account for charge cooling due to pilot-fuel vaporization, the temperatures of n-heptane-NG-air mixtures for various NG and n-heptane concentrations (corresponding to different spatial locations within the pilot-fuel jet) are computed assuming adiabatic mixing, accounting for both the sensible enthalpy and latent heat of vaporization of n-heptane. The homogenous reactor models use the Lawrence Livermore detailed *n*-heptane mechanism version 3.1 [28,29], which also includes chemistry for the methane, ethane, and propane of the synthetic NG. Ignition delay times (to second-stage ignition) are computed based on the inflection point in the temperature profile. The homogeneous reactor model only accounts for the chemical induction portion of the in-cylinder processes, as it is assumed that the reactor is perfectly mixed and does not interact with other local mixtures.

Results and Discussion

Natural Gas Fuel Infrared Imaging

A simulated emission spectrum of methane (mole fraction $X_{CH4} = 0.01$) at characteristic TDC conditions (800 K, 28.37 bar and 2.1 cm path length) using the spectroscopic parameters from the HITRAN database [30] is shown in Figure 2 along with the transmission cut-off wavelengths of various IR BPFs. Further details on simulating the molecular emission spectrum of methane using the HITRAN database can be found elsewhere [31]. The observed emission spectrum is dominated by the C-H vibrational stretch band (symmetric stretching:

2936 cm^{-1}; asymmetric stretching: 2853 cm^{-1}). Figure 2 also shows the correlation between the integrated emission intensity and the methane mole fraction (X_{CH4}), which is used to quantify in-cylinder NG concentration. At higher methane concentration ($X_{CH4} > 0.2$), the emission intensity essentially reaches blackbody levels resulting in a saturation effect. However, due to the fairly low operating equivalence ratios used in this study ($X_{CH4} \leq 0.05$ for $\phi_{NG} \leq 0.5$), the correlation falls in the more linear regime. This allows for accurately quantifying in-cylinder NG concentration using IR imaging within 2% of the actual values estimated from direct mass-flow meter based measurements. Calibration curves correlating IR intensity to known in-cylinder NG concentrations were obtained using a pre-calibrated, in-cylinder, sidewall mounted, NG direct injector (shown in the schematic layout in Figure 1). Direct NG injections were performed early in the compression stroke to yield a fairly homogenous mixture. Under such conditions, the IR emission using the NG fumigation strategy can be directly compared with the IR signal from calibrated direct injection of NG, which allows for estimation of in-cylinder NG equivalence ratio. This approach is feasible only for early NG direct injections that allows for sufficient time for NG to mix and be compressed simultaneously with the intake air, thereby decoupling the temperature and concentration dependencies of NG IR intensity at TDC conditions that would occur for injections during the compression stroke.

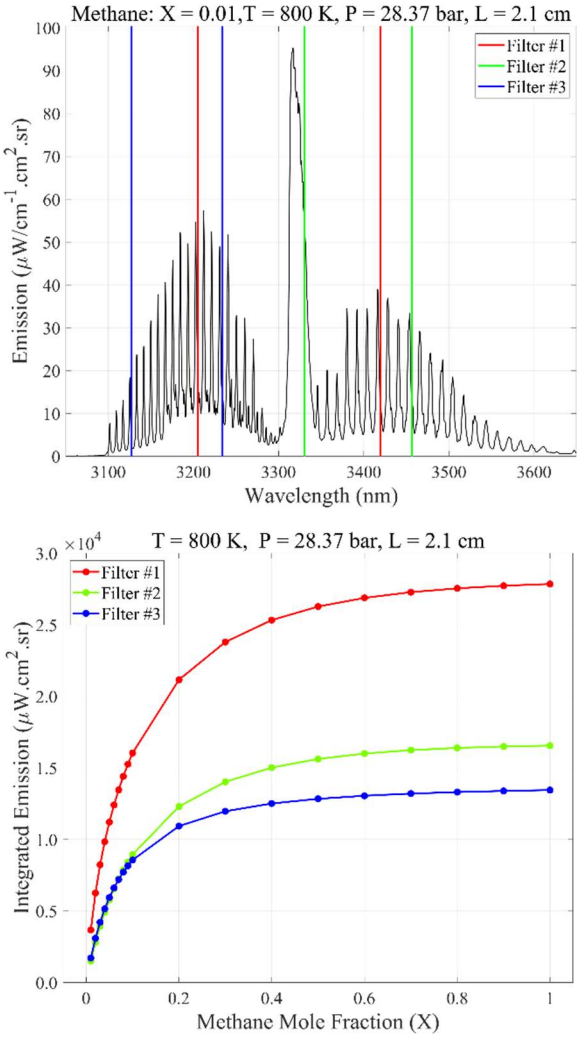

Figure 2. Top: HITRAN based simulated methane emission spectrum (X_{CH4} = 0.01 along with various IR filter cut-offs. Bottom: Integrated emission intensities for varying methane mole fraction for NG quantification at pressure P = 28.37 bar, temperature T = 800 K and path length L = 2.1 cm.

Because the optical engine is operated in a "9:1 skip-fire" mode, continuous injection of NG through the port injector during the motored cycles must be minimized as much as possible for safety considerations. Therefore, NG fumigation is activated only for a few cycles preceding the fired cycle. The minimum number of NG fumigation events that are necessary to create a well-premixed NG charge inside the cylinder is determined by changing the number of consecutive fumigation cycles while monitoring the variation in IR intensity at TDC for every cycle. The line plot at the top of Figure 3 shows the variation of normalized spatially integrated IR intensities at TDC for each cycle (including the first fumigation cycle) as the number of NG fumigation injections is varied. Sample IR images taken at TDC (360 CAD) for different cycles following the start of a 3-cycle NG fumigation event are also presented at the bottom of Figure 3. In cycles #4 and #5, the NG IR emission inside the cylinder is fairly uniform spatially (homogenous NG-air mixture) and of similar overall intensity. The small inhomogeneities observed in the IR images can be explained by relating this observation to a previous study [32] in a HCCI engine using a similar injection strategy that created a well premixed intake charge, which nevertheless, exhibited significant inhomogeneities in PLIF signal intensities at TDC. These inhomogeneities were due to natural thermal stratification and turbulent structures in the bulk gas rather than variations in the fuel-air mixture. Thus, minor spatial intensity variations observed in the IR images are most likely due to temperature inhomogeneity caused by the "scooping" of the relatively cool thermal boundary layer into the core gases [32] rather than mixture inhomogeneity. The line plots in Figure 3 shows that increasing the number of injected cycles beyond three maintains a relatively constant IR intensity (amount of NG at TDC) in later cycles. Based on this approach, a minimum of 3 injections are required to maintain quasi-steady in-cylinder NG concentration through the motor and fire cycles. However, for all results presented in this study, a 4-cycle (cycles #1 to #4) NG fumigation strategy is used, with cycle #6 used as fired cycle in the 9:1 skip-fire pattern. This approach minimizes the use of NG by a factor of 2.5, which reduces the risk of combustible mixture ignition in the exhaust plenum.

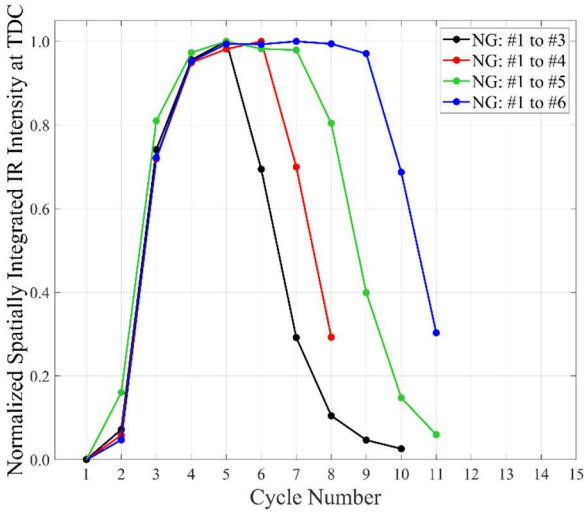

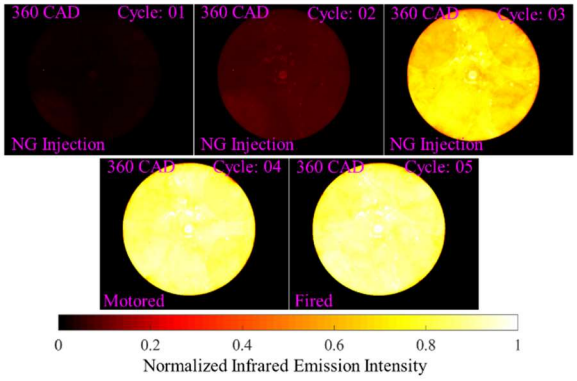

Figure 3. Top: Normalized spatially integrated in-cylinder NG IR emission intensity (related to NG concentration) with fumigation injections during cycles indicated in the legend. Bottom: NG IR emission images at TDC for fumigation injections during cycles #1 to #3.

Effect of Natural Gas on Pilot-Fuel Autoignition Characteristics

Cylinder Pressure and Apparent Heat Release Rate

The effects of NG concentration on the measured cylinder pressure and the calculated AHRR are shown in Figure 4 and Figure 5. Figure 4 shows that the peak cylinder pressure gradually rises with increasing NG concentration, from 35 bar for pilot-fuel only combustion to 40 bar for combustion of the highest premixed NG concentration tested (ϕ_{NG} = 0.5), i.e., a 14% increase in peak pressure for a four-fold increase (1.65 bar to 6.85 bar) in the corresponding gIMEP. This minimal increase in peak pressure despite a substantial increase in the total fueling rate is due to the inhibitive effect of NG on the ignition of the pilot-fuel, which leads to later ignition and timing of the pressure-peak. The combustion phasing is also delayed and the burn duration is extended which ultimately results in lower closed cycle efficiency due to the reduced effective expansion ratio [33].

The AHRR curves shown in Figure 5 exhibit the characteristic two-stage autoignition behavior for the diesel-like n-heptane pilot-fuel, even in the presence of NG. For all experimental conditions, the distinct drop in the AHRR below 0 J/ºCA starting at 350 CAD is due to evaporative cooling by the pilot-fuel spray. The low-temperature heat release (LTHR) pushes the AHRR above zero between 355 and 360 CAD, depending on ϕ_{NG}. Once the AHRR peaks during LTHR, it then drops to near zero, after which it increases more rapidly due to HTHR reactions. The relative onset, duration (shape), and peak AHRR during the LTHR and HTHR depend on the in-cylinder NG concentration. The relatively sharp and symmetric shape of the AHRR curve in the absence of NG suggests that majority of the heat release is primarily due to premixed autoignition of the pilot-fuel (very little mixing-controlled combustion) and the combustion event is completed within a few ºCA as the AHRR drops back to near zero levels quickly [23]. However, as the premixed NG concentration is increased, the HTHR becomes less symmetrical, characterized by a relatively long, increasingly prominent tail that involves one or more of mixing-controlled combustion, sequential autoignition of NG, and turbulent-flame propagation through the NG. Two competing effects appear to govern the combustion process. On one hand, a longer ignition delay dilutes the pilot-fuel and increases the amount of NG entrained resulting in higher peak heat release, while on the other hand increased NG entrainment and pilot-fuel dilution reduces reactivity further prolonging the pilot-fuel ignition delay. A peak AHRR of 366 J/ºCA at ϕ_{NG} = 0.3 suggests that the inhibitive effect of NG on pilot-fuel autoignition chemistry is balanced by the associated increase in mixing time available.

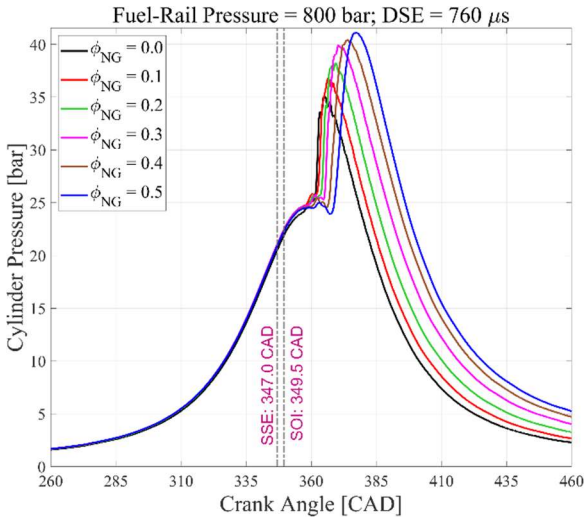

Figure 4. Cylinder pressure for various premixed natural gas concentrations (ϕ_{NG}). Pilot fuel injection parameters: Fuel-rail pressure = 800 bar, DSE = 760 µs.

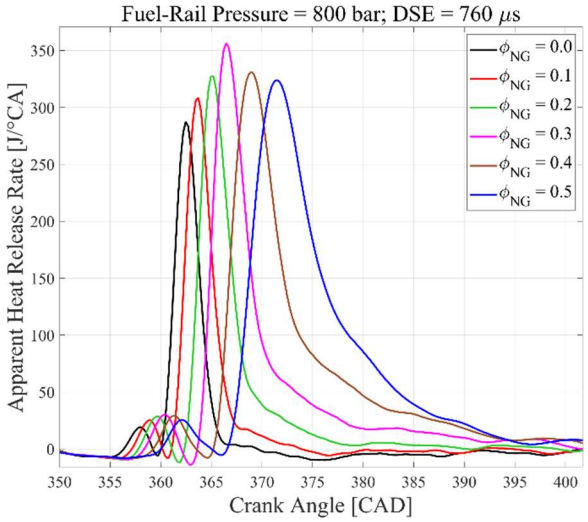

Figure 5. Apparent heat release rates (AHRR) for various premixed natural gas concentrations (ϕ_{NG}). Pilot fuel injection parameters: Fuel-rail pressure = 800 bar, DSE = 760 µs.

Ignition Delay

The dependence of first- and second-stage ignition delay of the pilot-fuel jet on the NG concentration is shown in Figure 6. The first- and second-stage ignition delays plotted in Figure 6 are the time between SOI and the crossing of 5 J/ºCA for the LTHR and HTHR. The error bars indicate one standard deviation variation from cycle to cycle.

In general, irrespective of the pilot-fuel injection parameters, the increasing NG concentration increases the ignition delay of the pilot-fuel quite significantly (up to 55% increase for ϕ_{NG} = 0.5). The ignition delay increase is nearly linear with ϕ_{NG}, which is in good agreement with existing literature [1,3,4,7,14,15]. The observed increase in ignition delay is predominantly attributed to the inhibition of low-

temperature pilot-fuel ignition chemistry by NG, and to lesser degrees, changes in the compressed-gas temperature at SOI resulting from changes in the mixture specific-heat ratio and lower oxygen concentration due to dilution of air by NG [13-15].

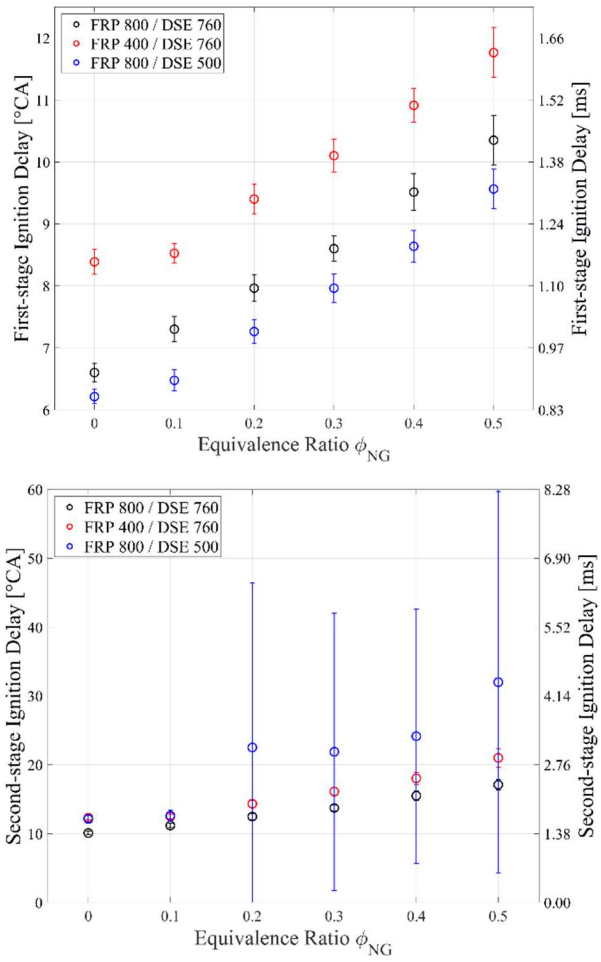

Figure 6. First- (top) and second-stage (bottom) ignition delays for various premixed NG concentrations (ϕ_{NG}). Pilot-fuel injection parameters (fuel-rail pressure FRP and duration of solenoid energizing DSE) are indicated in the legend. Error bars indicate one standard deviation of cycle-to-cycle variations.

For constant DSE (760 µs), higher pilot-fuel rail pressure (800 bar compared to 400 bar) increases the injected mass of pilot-fuel, enhances mixing and spray penetration rate, and has shorter ignition delays. For constant injected pilot-fuel mass, however, the 800 bar rail-pressure condition with 500-µs DSE had a shorter first-stage ignition delay compared to the 400-bar rail-pressure, 760-µs DSE conditions, irrespective of the NG concentration. This is likely due to a stronger end of injection "entrainment wave" [34] for the higher rail-pressure condition that increases the mixing rate, creating more fuel-lean regions with shorter first-stage ignition delays [9,10,13-15]. However, despite these shorter first-stage ignition delays, the 800-bar, 500-µs DSE pilot-fuel injection also has the longest second-stage ignition delays and increasingly high cycle-to-cycle variability (indicated by the error bars) with increasing premixed NG concentration, which indicates the pilot-fuel mixture is approaching the threshold of being "too lean to autoignite".

High Speed Chemiluminescence Imaging

Image Processing

Quantitative and qualitative information about the spatial and temporal progress of autoignition of the pilot-fuel in the presence of NG and the subsequent progress of combustion of NG from scores of high-speed chemiluminescence images are distilled into one single plot [13] for each condition through image processing, as follows. Sector masks are overlaid on every snapshot from the high-speed images of both cool-flame and OH* chemiluminescence to isolate individual sprays, as illustrated at the top of Figure 7. False-color scales of blue for cool-flame and red for OH* are applied to the original grayscale images to aid visualization. Intensities along the azimuthal direction within these sectors are then extracted for various distances downstream of the injector to the cylinder wall. These intensities are averaged and normalized by the maximum intensity in the corresponding set of images for each ϕ_{NG} of each pilot-fuel-injection condition. This normalized azimuthally-averaged intensity is then plotted as a function of the distance from the injector and crank angle as filled color-contour plots at the bottom of Figure 7. Vertical slices in the contour plot represent the variation of normalized azimuthally-averaged chemiluminescence intensity radially outward from the injector, extracted from a single snapshot at a given time instant as indicated by the corresponding CAD. Cool-flame chemiluminescence images saturate (intensity counts: 4095) near the second-stage autoignition (HTHR) irrespective of NG concentration. Hence, to clearly highlight the spatial and temporal features during the LTHR evolution when the cool-flame chemiluminescence is well below saturation and to aid visualization, the cool-flame contour plots employ a color scheme with only 25% dynamic range: black through blue to white indicating regions where normalized azimuthally-averaged intensity varies from 0 (black) to 0.25 of full scale, and constant white above 0.25 of full scale (see adjoining color bar in Figure 7). For OH* chemiluminescence imaging, saturation is not an issue, so the false-color scheme spans the full intensity range. The maximum intensity is dependent on the NG concentration, however, so the intensity normalization for the contour plots is based on the maximum intensity over all ϕ_{NG} for a given pilot-fuel-injection condition: black through red to white indicating regions where normalized azimuthally-averaged intensity varies from 0 to full scale, as indicated in the adjoining color bar. This false-color scheme allows for comparison of OH* chemiluminescence intensities across various NG concentrations while still effectively highlighting the spatial and temporal features during the progress of HTHR. Further, to aid correlation of the chemiluminescence image intensities to the heat release data, the corresponding AHRR (shown in magenta) is superimposed on the contour plot. Key events such as SSE, SOI, EOI, start of LTHR and HTHR (based on AHRR data analysis) are also indicated in the contour plot for ease of comparison. There is a clear correlation between the timing (CAD) of the peak AHRR (LTHR and HTHR) and the corresponding maximum intensity from the high-speed cool-flame and OH* chemiluminescence images. Hence, it is reasonable to consider cool-flame and OH* chemiluminescence imaging as approximate indictors of LTHR (first-stage ignition) and HTHR (second-stage ignition) respectively for this particular operating condition.

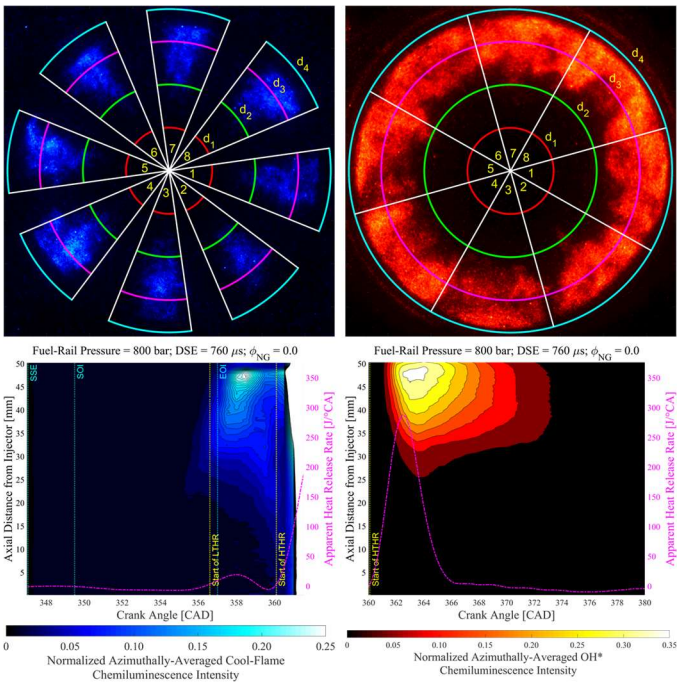

Figure 7. Top: Snapshots of high speed cool-flame (top left) and OH* (top right) chemiluminescence images showing the azimuthal sectoring scheme. Bottom: Contour plots of normalized azimuthally-averaged chemiluminescence intensities, superimposed with AHRR for LTHR (bottom left) and HTHR (bottom right) for n-heptane-only combustion (ϕ_{NG} =0). Pilot-fuel injection parameters: Fuel-rail pressure = 800 bar, DSE = 760 μs.

Spatial/Temporal Progression of First-Stage Ignition and Low-Temperature Heat Release

The spatial and temporal progression of first-stage LTHR (based on cool-flame chemiluminescence) of the n-heptane pilot-fuel jet (fuel-rail pressure: 800 bar, DSE: 760 μs) in the absence (pilot-fuel only) and presence of NG (ϕ_{NG} = 0.5) is summarized in the contour plots presented in Figure 8 and Figure 9, respectively. Salient snapshots from the high speed, cool-flame, broadband chemiluminescence revealing the differences in the autoignition characteristics of the pilot-fuel jet under these two conditions are also presented (in the middle and bottom rows of the two figures).

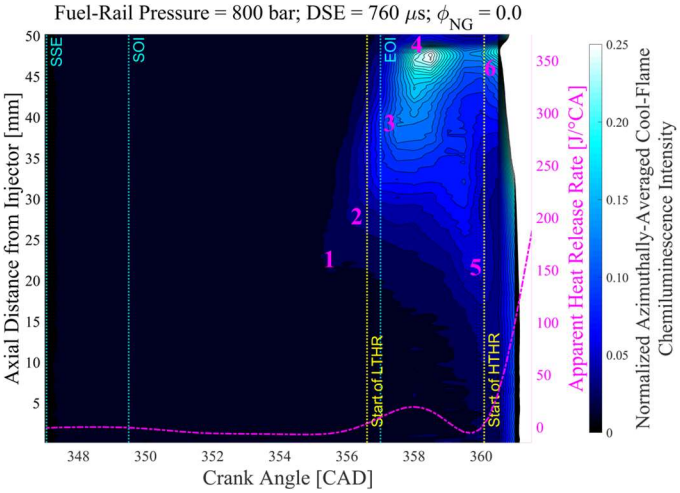

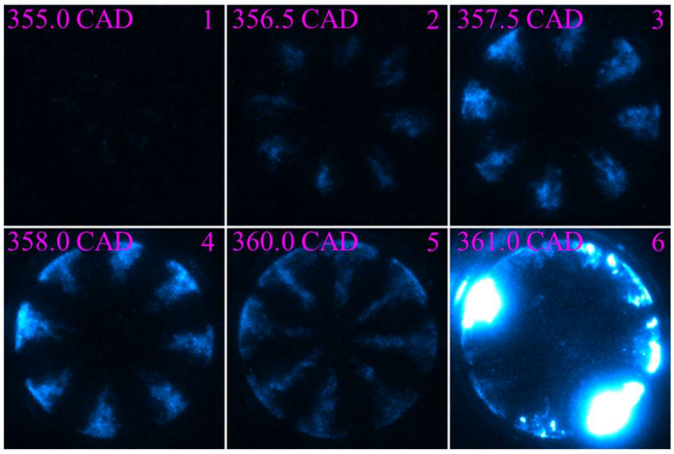

Figure 8. Contours of normalized azimuthally-averaged image intensities from cool-flame chemiluminescence imaging, superimposed with AHRR for n-heptane-only combustion. Middle and Bottom: Snapshots of representative cool-flame images at key timings during the LTHR. Numbers in the upper-right corner of the images are acquired at corresponding numbered timings in the contour plot.

In Figure 8, in the absence of NG (pilot-fuel only), the cool-flame chemiluminescence, taken as an indication of first-stage autoignition reactions according to the correlation with LTHR noted in Figure 7, initiates fairly close to the injector (20 mm downstream of the injector compared to the 50 mm bowl radius) at 355 CAD (image: 1), which is before EOI (negative ignition dwell). This first instance of chemiluminescence intensity exceeding the noise floor (signal to noise ratio exceeding 3) happens ~1 ºCA earlier than the computed start of LTHR as indicated in the contour plot. This temporal offset between cool-flame chemiluminescence and the start of LTHR evidenced by the AHRR is likely due in part to the simultaneous vaporization (endothermic) of the pilot-fuel offsetting the early LTHR (exothermic). The cool-flame chemiluminescence (LTHR) then proceeds toward the cylinder wall (image: 2) and reaches the cylinder wall at around 357.5 CAD (image: 3). The timing of the peak AHRR of the LTHR agrees well (within 0.5 ºCA) with maximum cool-flame chemiluminescence intensity observed at 358 CAD (image: 4). The EOI event is followed by a transient period of increased entrainment (entrainment wave) which increases mixing rates by up to a factor of three [34,35]. This results in faster progressive leaning-out of the mixture in the wake region of the pilot-fuel jet, creating fuel-lean regions near the injector. Hence, first-stage ignition tends to proceed upstream toward the injector (image: 5) as low temperature autoignition reactions are favored by hotter gases at lean conditions [9,10,13-15]. This is immediately followed by the appearance of multiple local hot-spots (indicated by regions of saturation) distributed near the cylinder wall (image: 6), which indicate transition to second-stage ignition.

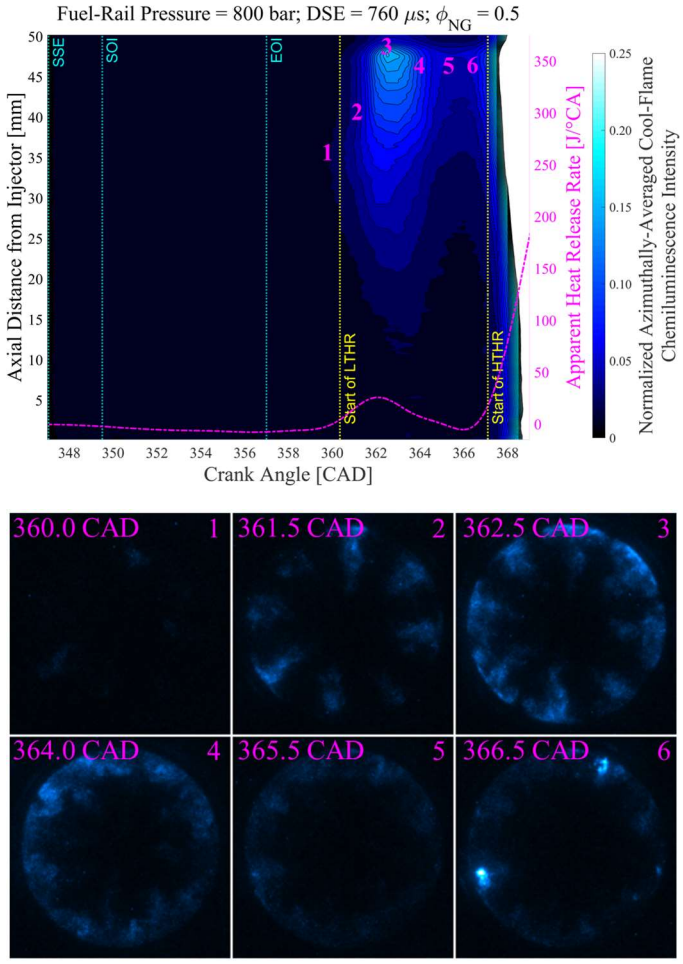

Figure 9. Top: Contours of normalized azimuthally averaged image intensities from cool-flame chemiluminescence imaging, superimposed with AHRR for n-heptane combustion in the presence of NG (ϕ_{NG} = 0.5). Middle and Bottom: Snapshots of representative cool-flame images at key timings during the LTHR. Numbers in the upper-right corner of the images are acquired at corresponding numbered timings in the contour plot.

Figure 9 shows that in the presence of NG (ϕ_{NG} = 0.5), due to the inhibitive effect of NG on the pilot-fuel autoignition chemistry, cool-flame chemiluminescence appears later. Due to the increased mixing time, the first-stage autoignition reactions tend to initiate further downstream of the injector (35 mm downstream of the injector) at 360 CAD (image: 1), much later than EOI (positive ignition dwell). This first occurrence of chemiluminescence agrees very well with the computed start of LTHR as indicated in the contour plot, partly due to the increased time available resulting in sequential occurrence of pilot-fuel vaporization followed by LTHR as opposed to their simultaneous and offsetting occurrence in the absence of NG as describe earlier. As in the previous case, the cool-flame chemiluminescence advances toward and reaches the cylinder wall at around 361.5 CAD (image: 2). However, there is no discernible progress of the cool-flame chemiluminescence upstream toward the injector as observed in the previous case, as the fuel-mixture close to the injector has leaned out considerably due to greater time available for mixing, resulting in an excessive first-stage ignition delay in the presence of NG [13-15]. Instead, the peak LTHR (maximum chemiluminescence intensity at 362.5 CAD: image: 3) is followed by a relatively long period (~4 ºCA) of reduced chemical reactivity (reducing chemiluminescence intensity: images: 4 and 5) before the appearance of relatively fewer local hot-spots near the cylinder wall (image: 6), signifying the start of second-stage, autoignition reactions. Notably, the timing of the peak LTHR matches within 1 ºCA, the maximum intensity from cool-flame chemiluminescence imaging.

Spatial/Temporal Progression of Second-Stage Ignition and High-Temperature Heat Release

The spatial and temporal progression of HTHR (based on OH* chemiluminescence imaging) of the n-heptane pilot-fuel jet (fuel-rail pressure: 800 bar, DSE: 760 μs) in the absence (pilot-fuel only) and presence of NG (ϕ_{NG} = 0.5) is summarized in the contour plots presented at the top of Figure 10 and Figure 11. Salient snapshots from the high-speed OH* chemiluminescence imaging revealing the differences in the progress of combustion of the pilot-fuel jet under these two conditions are also presented in the middle and bottom rows of the two figures.

Comparing the contour plots and images presented in Figure 8 with Figure 10 as well as Figure 9 with Figure 11, the temporal and spatial locations of the local hot spots in the cool-flame chemiluminescence images (image: 6in Figure 8 and Figure 9) coincide well (temporally within ~1 CAD, spatially within ~5 mm in terms of axial location) with the first occurrence of OH* chemiluminescence (image: 1in Figure 10 and Figure 11), even though the two imaging datasets are from separate experimental runs.

Figure 10 shows that in the absence of NG (pilot-fuel only), the second-stage ignition initiates fairly close to the cylinder wall on one or a few of the pilot-fuel jets nearly simultaneously at 361 CAD (image: 1) and rapidly progresses (within ~1 ˚CA) to all eight jets (image: 2). A rapid advancement of mixing-controlled/sequential-autoignition follows (images: 3 - 6). Emission here tends to be localized to the outer 50% of the combustion chamber bore and is completed in a relatively short duration (~10 CAD) for the short pilot-fuel injections (DSE: 760 μs) used here. Again, the timing of the peak AHRR of the HTHR agrees reasonably well with maximum chemiluminescence intensity observed at 363.5 CAD (image: 3).

Figure 11 shows that in the presence of NG (ϕ_{NG} = 0.5), the pilot-fuel jet experiences significantly longer second-stage ignition delays. Compared to Figure 10, the second-stage ignition kernels are formed much later at 367.5 CAD (image: 1) and spread to all eight jets at a slower rate (~2.5 CAD) (image: 2). Furthermore, there are stark differences in the progression of combustion in the presence of NG. First, the combustion is not confined to the boundary of the pilot-fuel jet due to the flammability of premixed NG-air outside the pilot jet. These regions are capable of sustaining a turbulent flame propagation and/or sequential autoignition almost throughout the entire cylinder. Second, the regions of most intense 310-nm emission remain close to the cylinder wall but lower intensity extends farther upstream in the jets towards the center of the cylinder (images: 3 and 4). Finally, the burn durations are much longer (~20 ºCA) as indicated by the AHRR plot and the residual 310-nm emission intensities during late cycle burn (images: 5 and 6). In the presence of NG, the maximum recorded 310-nm emission intensities are up to three times higher than the corresponding intensities recorded in the absence of NG. This increase in intensity is at least in part due the increasing soot luminosity rather than increasing OH* chemiluminescence, as the timing of this maximum intensity coincides well with the mixing-controlled phase of combustion [36]. Due to the increased availability of locally rich mixtures as a result of reduced oxygen concentration caused due to dilution of air by NG, in-cylinder soot formation appears to be enhanced, which interferes with OH* chemiluminescene imaging, resulting in higher observed 310-nm emission intensities.

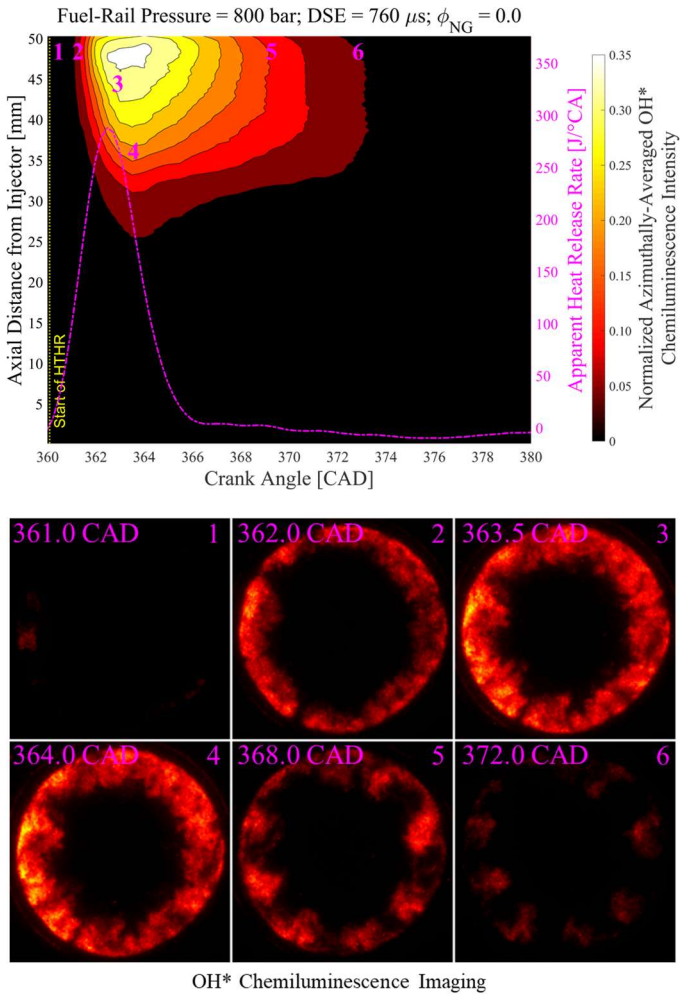

Figure 10. Top: Contours of normalized azimuthally-averaged image intensities from OH* chemiluminescence imaging, superimposed with AHRR for n-heptane only combustion. Middle and Bottom: Snapshots of representative OH* images at key timings during the HTHR. Numbers in the upper-right corner of the images are acquired at corresponding numbered timings in the contour plot.

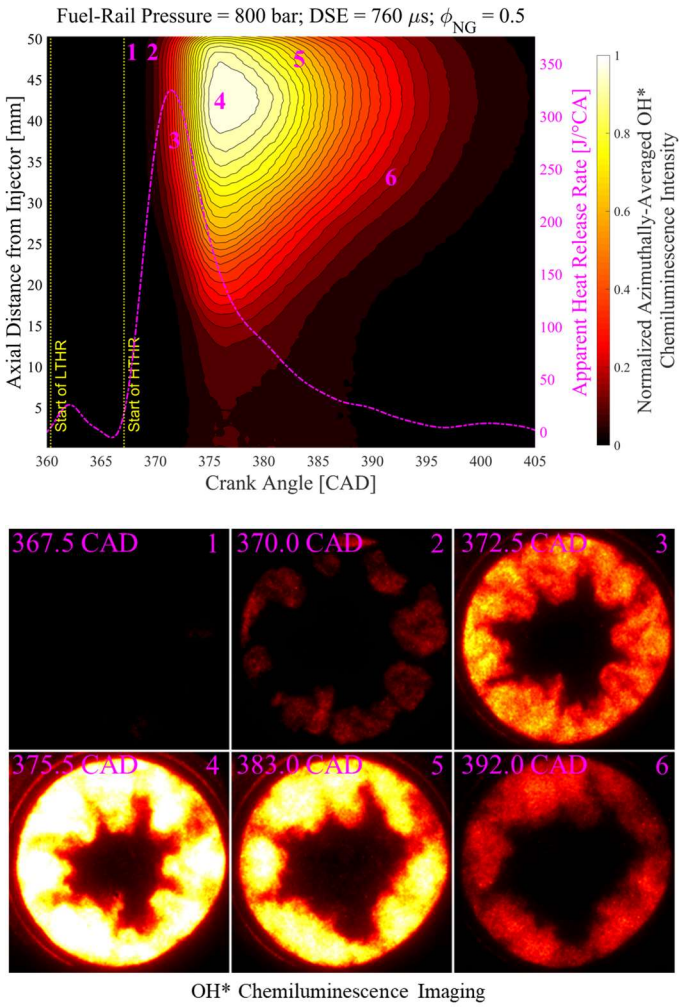

Figure 11. Top: Contours of normalized azimuthally-averaged image intensities from 310-nm emission imaging (OH* chemiluminescence and/or soot luminosity), superimposed with AHRR for n-heptane combustion in the presence of NG (ϕ_{NG} = 0.5). Middle and Bottom: Snapshots of representative images at key timings during the HTHR. Numbers in the upper-right corner of the images are acquired at corresponding numbered timings in the contour plot.

The combined spatial and temporal progress of two-stage ignition (LTHR and HTHR) of the n-heptane pilot-fuel jet (fuel-rail pressure: 800 bar, DSE: 760 μs) in the presence of varying NG concentrations from ϕ_{NG} = 0.0 to 0.5 in steps of 0.1 ϕ units is summarized in the contour plots presented in Figure 12. The rightward shift in the contours with increasing ϕ_{NG} reflects the increasingly inhibitive effect of NG on the first- and second-stage ignition. The first-stage ignition is delayed, and the dwell between first- and second-stage ignitions also increases. The spatial progress of the two-stage ignition also gradually evolves between the ϕ_{NG} = 0 and ϕ_{NG} = 0.5 conditions already discussed above. For ϕ_{NG} > 0.2, the OH* chemiluminescence contours extend closer to the center of the cylinder, possibly due to partial and/or sustained turbulent flame-propagation with increasing flame speed throughout the cylinder. Further, as the NG concentration is increased, the peak OH* chemiluminescence also increases. As described above, this increase is most likely due to progressively higher overall equivalence ratios resulting in increased in-cylinder soot formation, whose luminosity near 310 nm interferes with the OH* chemiluminescence. This also causes an increasing discrepancy between the timing of maximum HTHR and the maximum chemiluminescence intensity.

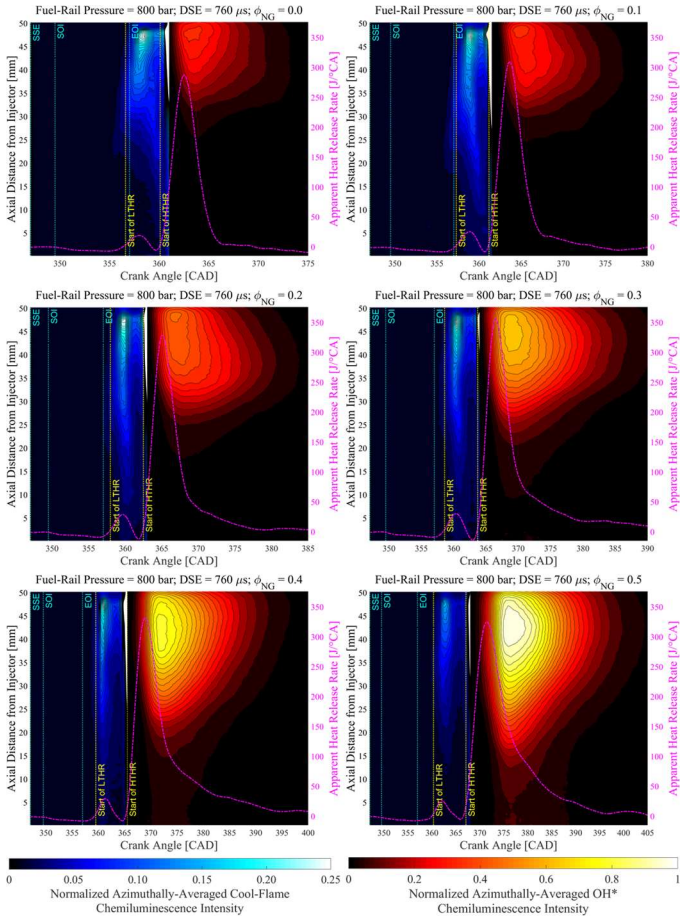

Figure 12. Contours of normalized azimuthally averaged image intensities from cool-flame chemiluminescence (shown in blue) and 310-nm emission from OH* and/or soot luminosity (shown in red) superimposed with AHRR for varying natural gas concentrations.

Combustion Duration and Phasing

The effect of NG concentration on the overall combustion duration is shown in Figure 13. Combustion duration is defined in two different ways. First, it is defined according to a conventional 10% to 90% of cumulative heat release (time-integrated AHRR). As shown in Figure 14, the 10% cumulative heat release threshold of this conventional definition occurs after the LTHR, however, so it does not capture changes in the dwell between first- and second-stage ignition. In an attempt to capture the increase in dwell between first- and second-stage ignition, an alternative definition based on the time between AHRR crossings of a 5 J/ºCA threshold is also calculated. We selected the 5 J/ºCA threshold based on inspection of the AHRR curves, placing it as high as possible while still being crossed during the LTHR for all conditions. The first upward crossing of the 5 J/ºCA threshold defines the start of combustion (SOC), while the last downward crossing of the threshold defines the end of combustion (EOC).

Combustion durations using both definitions are plotted in Figure 13. Due to the relatively slow energy release during the LTHR and the long late-cycle burn in the presence of NG, combustion durations computed as the time difference between SOC and EOC are roughly twice as long as the conventional 10% to 90% cumulative heat release. This difference is captured well in the combustion-phasing characteristics presented in Figure 14 for varying NG concentrations for fixed n-heptane pilot-fuel injection parameters (fuel-rail pressure: 800 bar, DSE: 760 μs).

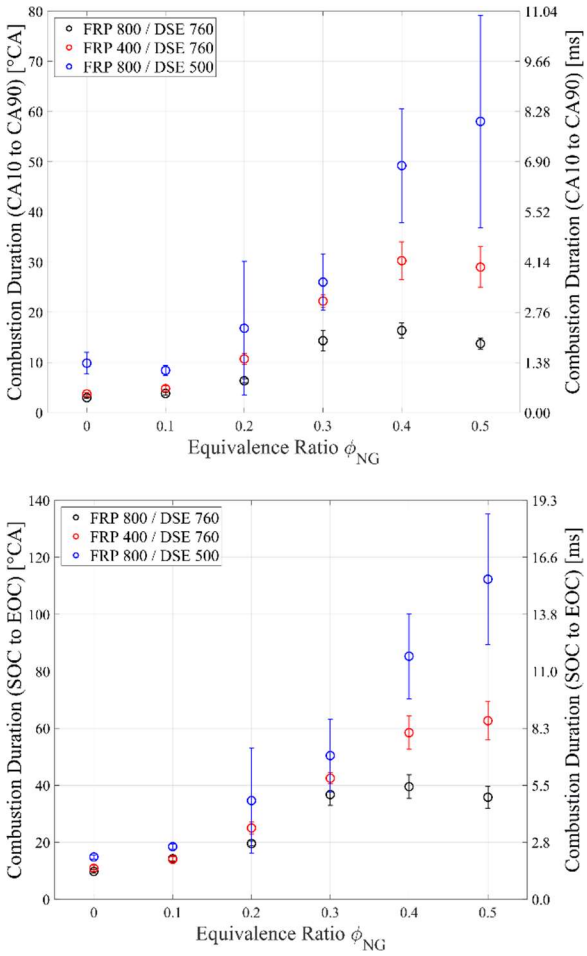

Figure 13. Combustion duration based on thresholds of either 10% to 90% cumulative heat release (top) or 5 J/°CA of AHRR (bottom) for various premixed natural gas concentrations (ϕ_{NG}). Pilot-fuel injection parameters (fuel-rail pressure FRP and duration of solenoid energizing DSE) are indicated in the legend. Error bars indicate one standard deviation of cycle-to-cycle variation.

Figure 13 shows a fairly linear increase in either definition of the combustion duration with NG concentration for $\phi_{NG} \leq 0.3$, irrespective of the pilot-fuel injection parameters. For $\phi_{NG} \geq 0.3$, the combustion duration trends depend on the pilot-fuel injection parameters. For the 500-μs DSE pilot-fuel jet at 800-bar rail pressure, the combustion durations continue to increase with NG concentration for $\phi_{NG} \geq 0.3$. For the other two conditions with longer DSE (760 μs) or with lower fuel-rail pressure (400 bar), the combustion durations change much less for $\phi_{NG} \geq 0.3$ than for $\phi_{NG} \leq 0.3$. In addition to continued combustion duration increase for $0.3 \leq \phi_{NG} \leq 0.5$, the 500-μs DSE pilot-fuel jet at 800-bar rail pressure also exhibits high cycle-to-cycle variability in the combustion durations, as indicated by the spans of the error bars, which represent one standard deviation. This increasing variability may be due to combined effects of an earlier onset of first-stage ignition due to increased fuel-air mixing after EOI by the entrainment wave, and/or the chemically inhibitive effect of NG increasing the dwell between first- and second-stage ignitions. This increases the variability in the location and the number of ignition kernels responsible for initiating second-stage HTHR, thereby

resulting in much longer combustion durations and poor combustion phasing.

Returning to Figure 14, one notable feature in the cumulative heat release merits discussion. At low NG concentrations (ϕ_{NG}), due to the relatively long time available for mixing, the majority of the heat release is during the premixed combustion of the pilot fuel and entrained NG, as indicated by the steep slope of the cumulative heat release curve after the low LTHR step. As the NG concentration is increased, this slope gradually decreases, indicating a more sustained heat release as the imaging results show that more NG appears to burn in a sequential autoignition and/or turbulent flame-propagation mode in addition to the combustion of pilot-fuel and entrained NG in a more pre-mixed and rapid-autoignition mode.

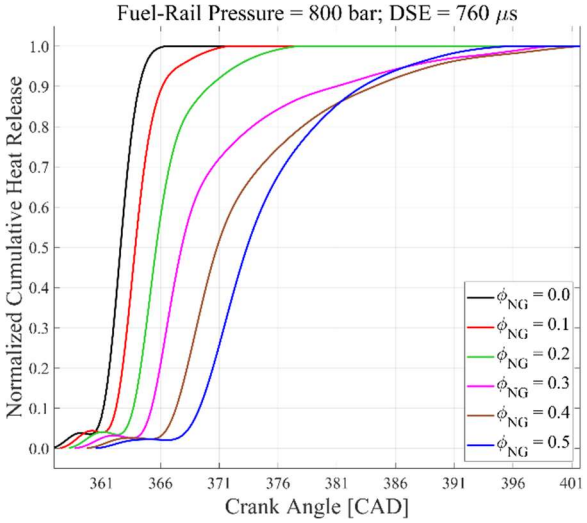

Figure 14. Normalized cumulative heat release for various premixed natural gas concentrations (ϕ_{NG}). Pilot fuel injection parameters (fuel-rail pressure and DSE) are indicated above the plot.

Chemical Kinetics Simulations

Figure 15 shows 0-D simulation predictions of time-resolved temperature profiles for stoichiometric n-heptane (calculated based on n-heptane and oxygen concentrations only) in various concentrations of NG (with ϕ_{NG} based on the NG and oxygen concentrations only). The predicted temperature profiles in the reactor exhibit the typical two-stage ignition behavior, characteristic of long-chain hydrocarbons like n-heptane. The computed second-stage ignition delays for various NG concentrations over a range of n-heptane pilot-fuel concentrations are shown in Figure 16. Low-temperature first-stage ignition reactions are favored by hotter gases at very lean conditions [9,10,13-15], while the most reactive mixtures for high-temperature second-stage ignition are slightly fuel-rich. Even though the 0-D model does not account for mixing, the range of predicted ignition delays encompass the experimentally measured values.

The simulations predict that NG has an increasingly significant inhibition effect on the autoignition chemistry of the n-heptane pilot-fuel, as indicated by the increasing ignition delays and the slight shift in the most-reactive mixture fraction toward progressively richer mixtures. This increase in ignition delay with increasing ϕ_{NG} is likely due to the combination of reduced oxygen concentration, increased mixture thermal capacity, and NG acting as a radical sink. However, the observed increase in the computed and calculated ignition delay times with increasing ϕ_{NG} is considerably more pronounced than the established empirical relation (ID ~ $[O_2]^{-1}$) between ignition delay and oxygen concentration [37]. Though the simulations predict a slightly richer n-heptane mixture as the new potential ignition site in the presence of NG, its physical availability may not be guaranteed due to the longer time for mixing to leaner mixtures as result of increasing ignition delays. The spatial location of this physically available most-reactive mixture will determine the subsequent combustion characteristics. Thus, for the shorter pilot-fuel injection duration typical of dual-fuel combustion, the interplay among the inhibitive effect of NG on the autoignition chemistry of the pilot-fuel, greater entrainment of natural gas mixture into the pilot-fuel jet due to the increased ignition delay time, and the transient increase in entrainment from the entrainment wave after EOI, all affect the spatial location of ignition and subsequent combustion.

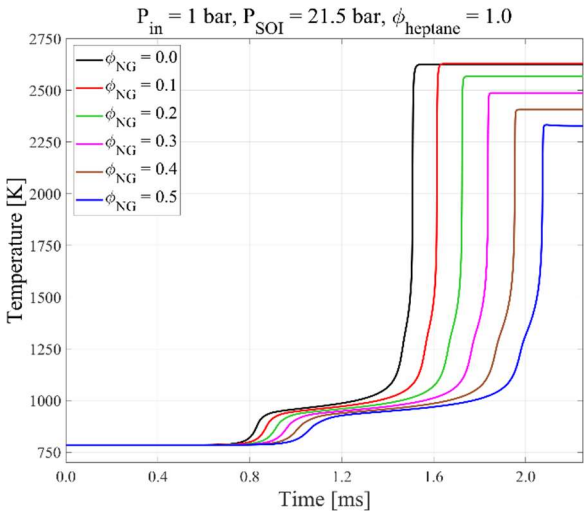

Figure 15. Predicted gas temperatures of 0-D chemical kinetics simulations at various natural gas concentrations (ϕ_{NG}) for two-stage autoignition of stoichiometric n-heptane.

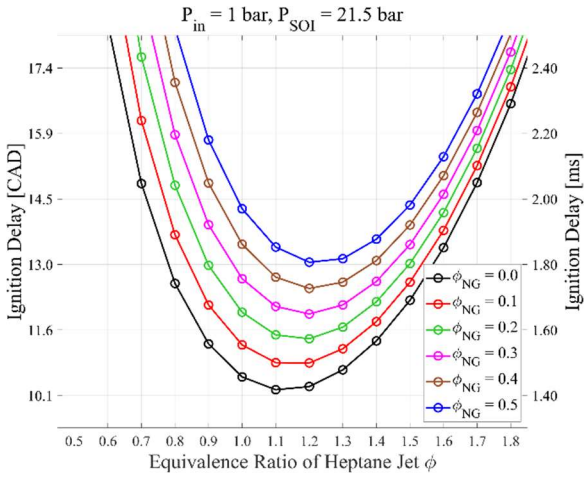

Figure 16. Predicted second-stage ignition delay of 0-D chemical kinetics simulations.

Further insight into the combination of chemistry and mixing might be gained through 1-D reacting jet simulations, perhaps using a flamelet-type model to account for mixing as ignition reactions proceed. Such simulations would likely better predict the combined effects of autoignition chemistry and mixing to identify the factors that control the onset of ignition and subsequent combustion, both the timing (e.g.,

for combustion phasing) and the spatial location (e.g., for affecting heat transfer to walls or otherwise affecting stratification). For example, guidance on how to adjust injection parameters to offset the changes in autoignition chemistry might be a valuable tool for combustion design.

Conclusions

The underlying processes governing the spatial and temporal progression of two-stage autoignition of a diesel-fuel surrogate, n-heptane, in a lean-premixed charge of synthetic NG and air are investigated in an optically accessible heavy-duty diesel engine. The aim of this study is to improve understanding of the influence of engine operating parameters on pilot-fuel autoignition characteristics. Representative measurements with variation of pilot-fuel injection parameters (fuel-rail pressure and DSE) and premixed NG concentration (ϕ_{NG}) are presented. AHRR analysis is supplemented with optical imaging of three different natural emissions: IR emissions due to C-H stretch emission from compression-heated fuel for quantifying in-cylinder NG concentration, high-speed (15 kfps) cool-flame chemiluminescence to observe the temporal and spatial progression of first-stage ignition and LTHR, and OH* chemiluminescence to track the subsequent transition to second-stage ignition and HTHR. Interpretation of experimental observations is aided by 0-D chemical kinetics simulations using a homogenous reactor model.

Analysis of experimental results and simulation predictions support the following conclusions:

1. Increasing the premixed NG concentration prolongs the first- and second-stage ignition delays of the pilot-fuel due to a chemical inhibition effect.

2. Pilot-fuel injection parameters (fuel-rail pressure and DSE) have a significant effect on the on the ignition delay times and the subsequent combustion duration and combustion phasing for both pure n-heptane fuel and dual-fuel cases, indicating that mixing characteristics can be manipulated to control ignition and the progression of combustion.

3. A shorter pilot-fuel DSE yields an earlier onset of first-stage ignition independent of NG concentration, which is likely due to an earlier occurrence of EOI and the associated entrainment wave-induced transient mixing that results in earlier leaning out ($\phi\downarrow$) of the pilot-fuel jet creating mixtures that reach first-stage ignition sooner. The 800-bar, 500-µs DSE pilot-fuel jet has the shortest low-temperature ignition delay, 6.2 ºCA for $\phi_{NG} = 0$, and up to 9.5 ºCA for $\phi_{NG} = 0.5$, which is consistently around 2 ºCA shorter than the ignition delay times for the 400-bar, 760-µs DSE pilot-fuel jet that contained the same amount of pilot fuel.

4. The enhanced mixing for shorter pilot-fuel DSE however likely reduces the availability of more reactive mixture fractions ($\phi \sim 1$) required for high-temperature autoignition reactions, resulting in longer dwell between first- and second-stage ignition, and increased cycle-to-cycle variability in the second-stage ignition delay. The 800-bar, 500 µs pilot-fuel jet had the longest dwell, 6.0 ºCA for $\phi_{NG} = 0$ and up to 22.5 ºCA for $\phi_{NG} = 0.5$, which is 50 to 150% longer than the corresponding dwell times measured with the 400-bar, 760-µs DSE pilot-fuel jet.

5. The longer dwell period for the shorter DSE pilot-fuel jet is further amplified due to reduction in the number of ignition kernels and a later onset at a location farther from the injector, closer to the cylinder wall. These trends are more pronounced with increasing NG concentrations. At $\phi_{NG} = 0.5$, the 800-bar, 500-µs DSE pilot-fuel jet has only 1 to 3 ignition kernels located near the bowl wall as opposed to more distributed ignition of all 8 jets for the 400-bar, 760-µs DSE pilot-fuel jet.

6. The slower formation of ignition kernels for the shorter DSE pilot-fuel jet results in a slow apparent flame propagation in fuel-lean NG mixtures, resulting in relatively long combustion durations. The 800-bar, 500-µs DSE pilot-fuel jet has the longest burn duration, 9.8 ºCA for n-heptane only and as long as 58.0 ºCA for $\phi_{NG} = 0.5$, which is approximately twice as long as the corresponding combustion durations measured with the 400-bar, 760-µs DSE pilot-fuel jet.

Thus for shorter pilot-fuel injection durations, the timing of the EOI entrainment wave and the associated transient mixing enhancement increasingly affects autoignition characteristics (first- and second-stage ignition delay and the dwell between them) and subsequent combustion phasing, which is further amplified in the presence of premixed NG. Fortunately, these effects might be mitigated by adjusting the injection parameters to use mixing to offset the changes in ignition chemistry to achieve desired combustion phasing and location, which can be a valuable tool for combustion design to improve fuel efficiency or reduce noise or perhaps even reduce heat transfer losses by locating early combustion away from in-cylinder walls.

References

1. Liu, J., et al., *Effects of pilot fuel quantity on the emissions characteristics of a CNG/diesel dual fuel engine with optimized pilot injection timing.* Applied Energy, 2013. **110**: p. 201-206.
2. Rochussen, J., J. Yeo, and P. Kirchen, *Effect of Fueling Control Parameters on Combustion and Emissions Characteristics of Diesel-Ignited Methane Dual-Fuel Combustion.* SAE Technical Paper, 2016-01-0792, 2016.
3. Schlatter, S., et al., *Experimental Study of Ignition and Combustion Characteristics of a Diesel Pilot Spray in a Lean Premixed Methane/Air Charge using a Rapid Compression Expansion Machine.* SAE Technical Paper, 2012-01-0825, 2012.
4. Schlatter, S., et al., *N-heptane micro pilot assisted methane combustion in a Rapid Compression Expansion Machine.* Fuel, 2016. **179**: p. 339-352.
5. Dronniou, N., et al., *Optical Investigation of Dual-fuel CNG/Diesel Combustion Strategies to Reduce CO2 Emissions.* SAE Technical Paper, 2014-01-1313, 2014.
6. Nithyanandan, K., et al., *An Optical Investigation of Multiple Diesel Injections in CNG/Diesel Dual-Fuel Combustion in a Light Duty Optical Diesel Engine.* SAE Technical Paper, 2017-01-0755, 2017.
7. Salaun, E., et al., *Optical Investigation of Ignition Timing and Equivalence Ratio in Dual-Fuel CNG/Diesel Combustion.* SAE Technical Paper, 2016-01-0772, 2016.
8. Borghesi, G., E. Mastorakos, and R.S. Cant, *Complex chemistry DNS of n-heptane spray autoignition at high pressure and*

intermediate temperature conditions. Combustion and Flame, 2013. **160**(7): p. 1254-1275.
9. Dahms, R.N., et al., *Understanding the ignition mechanism of high-pressure spray flames.* Proceedings of the Combustion Institute, 2017. **36**(2): p. 2615-2623.
10. Krisman, A., E.R. Hawkes, and J.H. Chen, *Two-stage autoignition and edge flames in a high pressure turbulent jet.* Journal of Fluid Mechanics, 2017. **824**: p. 5-41.
11. Skeen, S.A., J. Manin, and L.M. Pickett, *Simultaneous formaldehyde PLIF and high-speed schlieren imaging for ignition visualization in high-pressure spray flames.* Proceedings of the Combustion Institute, 2015. **35**(3): p. 3167-3174.
12. Karim, G.A., *Combustion in Gas Fueled Compression: Ignition Engines of the Dual Fuel Type.* Journal of Engineering for Gas Turbines and Power, 2003. **125**(3): p. 827-836.
13. Rajasegar, R., et al., *Influence of Pilot-Fuel Mixing on the Spatio-Temporal Progression of Two Stage Autoignition of Diesel-Sprays in Low-Reactivity Ambient Fuel-Air Mixture.* Proceedings of the Combustion Institute, 2020.
14. Niki, Y., et al., *Verification of diesel spray ignition phenomenon in dual-fuel premixed natural gas engine.* International Journal of Engine Research 2020.
15. Srna, A., et al., *Effect of methane on pilot-fuel auto-ignition in dual-fuel engines.* Proceedings of the Combustion Institute, 2019. **37**(4): p. 4741-4749.
16. Wong, Y.K. and G.A. Karim, *A Kinetic Examination of the Effects of Recycled Exhaust Gases on the Autoignition of Homogeneous N-Heptane-Air Mixtures in Engines.* SAE Technical Paper, 2000-01-2037, 2000.
17. Liu, Z. and G.A. Karim, *An Examination of the Ignition Delay Period in Gas-Fueled Diesel Engines.* Journal of Engineering for Gas Turbines and Power, 1998. **120**(1): p. 225-231.
18. Badr, O., G.A. Karim, and B. Liu, *An examination of the flame spread limits in a dual fuel engine.* Applied Thermal Engineering, 1999. **19**(10): p. 1071-1080.
19. Genzale, C.L., R.D. Reitz, and M.P.B. Musculus, *Optical Diagnostics and Multi-Dimensional Modeling of Spray Targeting Effects in Late-Injection Low-Temperature Diesel Combustion.* SAE Technical Paper, 2009-01-2699, 2009.
20. Dec, J.E., *A Conceptual Model of DI Diesel Combustion Based on Laser-Sheet Imaging*.* SAE Technical Paper, 970873, 1997.
21. Espey, C. and J.E. Dec, *Diesel Engine Combustion Studies in a Newly Designed Optical-Access Engine Using High-Speed Visualization and 2-D Laser Imaging.* SAE Technical Paper, 930971, 1993.
22. Heywood, J.B., *Internal combustion engine fundamentals*. 1988: New York : McGraw-Hill, [1988] ©1988.
23. Kokjohn, S.L., M.P.B. Musculus, and R.D. Reitz, *Evaluating temperature and fuel stratification for heat-release rate control in a reactivity-controlled compression-ignition engine using optical diagnostics and chemical kinetics modeling.* Combustion and Flame, 2015. **162**(6): p. 2729-2742.
24. Pickett, L.M., D.L. Siebers, and C.A. Idicheria, *Relationship Between Ignition Processes and the Lift-Off Length of Diesel Fuel Jets.* SAE Technical Paper, 2005-01-3843, 2005.
25. Siebers, D.L. and B. Higgins, *Flame Lift-Off on Direct-Injection Diesel Sprays Under Quiescent Conditions.* SAE Technical Paper, 2001-01-0530, 2001.
26. Anders, H., et al., *A Study of the Homogeneous Charge Compression Ignition Combustion Process by Chemiluminescence Imaging.* SAE Technical Paper, 1999-01-3680, 1999.
27. Dec, J.E., W. Hwang, and M. Sjöberg, *An Investigation of Thermal Stratification in HCCI Engines Using Chemiluminescence Imaging.* SAE Technical Paper, 2006-01-1518, 2006.
28. Mehl, M., et al., *Detailed Kinetic Modeling of Low-Temperature Heat Release for PRF Fuels in an HCCI Engine.* SAE Technical Paper, 2009-01-1806, 2009.
29. Mehl, M., et al., *Kinetic modeling of gasoline surrogate components and mixtures under engine conditions.* Proceedings of the Combustion Institute, 2011. **33**(1): p. 193-200.
30. Rothman, L.S., et al., *The HITRAN database: 1986 edition.* Applied Optics, 1987. **26**(19): p. 4058-4097.
31. Goldenstein, C.S., et al., *SpectraPlot.com: Integrated spectroscopic modeling of atomic and molecular gases.* Journal of Quantitative Spectroscopy and Radiative Transfer, 2017. **200**: p. 249-257.
32. Dec, J.E. and W. Hwang, *Characterizing the Development of Thermal Stratification in an HCCI Engine Using Planar-Imaging Thermometry.* SAE Technical Paper, 2009-01-0650, 2009.
33. Stanton, D.W., *Systematic Development of Highly Efficient and Clean Engines to Meet Future Commercial Vehicle Greenhouse Gas Regulations.* SAE Technical Paper, 2013-01-2421, 2013.
34. Musculus, M.P.B. and K. Kattke, *Entrainment Waves in Diesel Jets.* SAE International Journal of Engines, 2009. **2**(1): p. 1170-1193.
35. Musculus, M.P.B., et al., *End-of-Injection Over-Mixing and Unburned Hydrocarbon Emissions in Low-Temperature-Combustion Diesel Engines.* SAE Technical Paper, 2007-01-0907, 2007.
36. Huestis, E., P.A. Erickson, and M.P.B. Musculus, *In-Cylinder and Exhaust Soot in Low-Temperature Combustion Using a Wide-Range of EGR in a Heavy-Duty Diesel Engine.* SAE Technical Paper, 2007-01-4017, 2007.
37. Idicheria, C.A. and L.M. Pickett, *Ignition, soot formation, and end-of-combustion transients in diesel combustion under high-EGR conditions.* International Journal of Engine Research, 2011. **12**(4): p. 376-392.

Contact Information

Rajavasanth Rajasegar : Combustion Research Facility, Sandia National Laboratories, 7011 East Avenue, Livermore, CA, 94550, USA; rrajase@sandia.gov; +1-925-294-6401.

Acknowledgements

This research was sponsored by the U.S. Department of Energy (DOE) Office of Energy Efficiency and Renewable Energy (EERE). Optical engine experiments were conducted at the Combustion Research Facility of Sandia National Laboratories in Livermore, CA. Sandia National Laboratories is a multi-mission laboratory managed and operated by National Technology and Engineering Solutions of Sandia, LLC., a wholly owned subsidiary of Honeywell International, Inc., for the U.S. Department of Energy's National Nuclear Security Administration (NNSA) under contract DE-NA0003525. We gratefully acknowledge the contributions of Keith Penney and Dave Cicone for their assistance in developing research tools and maintaining the optical engine.

Definitions/Abbreviations

IC	Internal combustion
NOx	Nitrogen oxides
UHC	Unburned hydrocarbon

NG	Natural gas
IR	Infrared
LTHR	Low-temperature heat release
HTHR	High-temperature heat release
UV	Ultraviolet
BPF	Band-pass filter
FWHM	Full-width at half-maximum
HCCI	Homogeneous charge compression ignition
X	Mole-fraction
ϕ_{NG}	Premixed natural gas equivalence ratio
RPM	Rotations per minute
TDC	Top dead center
SSE	Start of solenoid energization
DSE	Duration of solenoid energization
SOI	Start of injection
EOI	Start of injection
ºCA	Degrees crank angle (interval/duration)
CAD	Crank-angle degrees (timing)
ID	Ignition delay
AHRR	Apparent heat release rate
gIMEP	Gross indicated mean effective pressure
SOC	Start of combustion
EOC	Start of combustion
0-D	Zero-dimensional